International Journal of Hydrogen Energy 231 (2026) 154877

Contents lists available at ScienceDirect

International Journal of Hydrogen Energy

journal homepage: www.elsevier.com/locate/he

Metal hydride-based hydrogen storage for fuel cell hybrid electric vehicles: numerical evaluation under real-world operating conditions

L. Bartolucci [a,*], E. Cennamo [a], S. Cordiner [a], V.K. Krastev [b], V. Mulone [a], A. Polimeni [a,**]

[a] Department of Industrial Engineering, Tor Vergata University of Rome, Via del Politecnico 1, 00133, Rome, Italy
[b] Department of Enterprise Engineering, Tor Vergata University of Rome, Via del Politecnico 1, 00133, Rome, Italy

ARTICLE INFO

Keywords:
Metal hydrides
Fuel cell hybrid electric vehicle
Sustainability
Micromobility

ABSTRACT

The work investigates the integration of metal hydride (MH) hydrogen storage systems in a fuel cell plug-in hybrid electric microcar, with emphasis on how thermal management and system operation affect vehicle-level performance. A comprehensive numerical framework is developed by embedding a one-dimensional MH model into a hybrid powertrain simulation environment. The effectiveness of natural convection, forced convection using fuel cell waste heat, and passive thermal buffering through phase change materials (PCMs) is assessed. Results indicate that natural convection cannot sustain hydrogen desorption, whereas forced convection enables a 40% increase in driving range relative to a battery-electric vehicle (BEV). The inclusion of PCMs allows hydrogen utilization up to 99% in dual-tank layouts. These improvements translate into a driving range of around 180 km —three times the baseline BEV—and a fuel cell energy contribution approaching 50%. Simulations under realistic urban driving cycles confirm the suitability of MH-based storage for micromobility applications.

Nomenclature

Abbreviations	
Abbreviation	Definition
BESS	Battery Energy Storage System
BEV	Battery Electric Vehicle
CFD	Computational Fluid Dynamics
DC	Direct Current
EMS	Energy Management System
FC	Forced Convection
FCHEV	Fuel Cell Hybrid Electric Vehicle
FCPHEV	Fuel Cell Plug-in Hybrid Electric Vehicle
FCS	Fuel Cell Stack
KPI	Key Performance Indicator
MH	Metal Hydride
NC	Natural Convection
PCI	Pressure-Composition-Isotherm
PCM	Phase Change Material
PEM	Proton Exchange Membrane
RE	Range Extender
SOC	State Of Charge
WMTC	World Motorcycle Test Cycle

(*continued on next column*)

(*continued*)

Symbols		
Symbol	Definition	Unit
E_a	Activation energy	kJ mol^{-1}
K_0	Arrhenius pre-exponential factor	s^{-1}
ρ	Density	kg m^{-3}
D	Diameter	m
k_{eff}	Effective thermal conductivity	W m^{-1} K^{-1}
C_{eff}	Effective volumetric heat capacity	J m^{-3} K^{-1}
H	Height	m
L_m	Latent heat of fusion	J kg^{-1}
f_L	Liquid fraction	–
m	Mass	kg
M	Molar mass	kg mol^{-1}
T_m	PCM melting temperature	K
ΔT	PCM melting temperature interval	K
ε	Porosity	–
r	Radial coordinate	m
ΔH	Reaction enthalpy of the metal hydride	J mol^{-1}
ΔS	Reaction entropy of the metal hydride	J mol^{-1} K^{-1}
c_p	Specific heat capacity	J kg^{-1} K^{-1}

(*continued on next page*)

This article is part of a special issue entitled: EFCHC25 conference (Iulianelli) published in International Journal of Hydrogen Energy.

* Corresponding author.
** Corresponding author.
E-mail addresses: lorenzo.bartolucci@uniroma2.it (L. Bartolucci), alessandro.polimeni@uniroma2.it (A. Polimeni).

https://doi.org/10.1016/j.ijhydene.2026.154877
Received 12 February 2026; Received in revised form 14 March 2026; Accepted 2 April 2026
Available online 7 April 2026

(*continued*)

T	Temperature	K
k	Thermal conductivity	$W\ m^{-1}\ K^{-1}$
t	Time	s
V	Volume	m^3

1. Introduction

The decarbonization of the transport sector, which accounts for approximately 24% of global CO_2 emissions, is a key challenge in the transition toward sustainable energy systems [1]. Road transport accounts for more than 70% of these emissions [2], with urban mobility playing a major role due to congestion, short trips, and frequent stop-and-go operation, which exacerbate energy inefficiencies and local pollution [3], [4], [5]. In this context, sustainable mobility evolved from a predominantly vehicle-centered perspective toward a system-level approach, in which energy carriers, storage technologies, and control strategies play a fundamental role alongside vehicle design [6], [7].

Electrification has emerged as a dominant pathway for reducing local emissions and primary energy use in urban transport [8]. However, the effectiveness of purely battery-electric solutions strongly depends on usage patterns and operational constraints, particularly for lightweight vehicles with limited onboard energy storage [9], [10]. These limitations are especially relevant in the micromobility sector, which is gaining increasing interest to efficiently address individual mobility problems in urban areas. For these vehicle categories, mass and volume constraints restrict battery size and, consequently, vehicle range.

Within this framework, hydrogen may be an efficient and complementary energy carrier, owing to its high gravimetric energy density and its compatibility with low-carbon energy pathways [11]. When integrated into Fuel Cell Hybrid Electric Vehicles (FCHEVs), hydrogen enables zero local emissions while extending vehicle range beyond what is typically achievable with Battery Electric Vehicles (BEVs) [12]. In FCHEVs, where propulsion power is supplied jointly by a Fuel Cell Stack (FCS) and a battery pack, the Energy Management Strategy (EMS) plays a critical role in allocating power between the two sources [13]. Several EMS approaches have been proposed in the literature, including the Range Extender strategy, identified by Bartolucci et al. [14] as particularly suitable for hybrid architectures. In particular, the battery acts as the primary energy source while the FCS operates intermittently to recharge it below a given State of Charge (SOC) threshold.

The effectiveness of these control strategies is inherently linked to the characteristics and dynamic behavior of the onboard hydrogen storage system. Conventional high-pressure hydrogen tanks, however, pose challenges due to their low volumetric energy density and energy-intensive compression, which are particularly restrictive for compact and lightweight vehicles [15]. In this respect, metal hydride-based hydrogen storage is a promising alternative, enabling solid-state hydrogen storage at relatively low operating pressures and offering enhanced intrinsic safety and system integration potential [16]. Nevertheless, hydrogen absorption and desorption processes in metal hydrides are governed by strongly coupled thermo-chemical processes [17]. The exothermic nature of absorption and the endothermic nature of desorption induce temperature gradients that directly affect reaction equilibrium and kinetics, potentially limiting hydrogen release and, in severe cases, interrupting hydrogen supply to the FCS.

For metal hydride-based storage systems, therefore, thermal management emerges as a key enabling factor. Several studies have demonstrated that inadequate heat removal or supply can severely degrade storage performance. Chung and Ho [18] showed that insufficient heat exchange leads to pronounced temperature gradients and slower reaction kinetics, while Nguyen and Shabani [19] reported reductions in storage efficiency of 10–20% and refueling times up to 4 times longer under poor thermal control. These findings highlight that metal hydride performance cannot be assessed independently from thermal management, particularly under dynamic operating conditions typical of vehicular applications. This issue has been further emphasized in recent reviews, such as that by Drawer et al. [20], which identify thermal management as a major barrier to the widespread adoption of metal hydrides.

Among the proposed thermal management solutions, Phase Change Materials (PCMs) have attracted growing interest as passive thermal buffers [21]. By storing and releasing thermal energy via latent heat during phase transitions, PCMs can mitigate temperature excursions within the metal hydrides during hydrogen absorption and desorption. As shown by Nyamsi and Tolj [22], heat generated during absorption can be partially stored in the PCM and subsequently reused during desorption, reducing the need for active thermal control. Several phase change materials have been investigated for thermal management of metal hydride storage systems. Organic PCMs such as paraffin waxes and fatty acids, inorganic salt hydrates, and high-temperature materials such as erythritol have been widely explored due to their suitable phase transition temperatures and high latent heat. These materials have been successfully integrated with $LaNi_5$-based or similar metal hydride systems to buffer the heat released during hydrogen absorption and to support desorption processes [23]. However, effective PCM integration requires careful material selection and system design. Nguyen and Shabani [19] identified key requirements for PCM suitability, including high latent heat, appropriate phase transition temperature, limited volumetric expansion, and sufficient thermal conductivity. Strategies such as incorporating expanded graphite have been proposed to enhance PCM thermal performance [24].

Beyond material properties, the amount and spatial distribution of PCM play a crucial role. El Mghari et al. [25] demonstrated that oversized or poorly coupled PCM layers may result in only partial utilization of the phase change process, emphasizing the need to balance thermal buffering capacity, added mass, and geometric constraints.

In this context, the coupled analysis of metal hydride storage and PCM-based thermal management becomes particularly relevant for vehicular applications. During hydrogen absorption, the strongly exothermic reaction generates significant heat that may increase the MH bed temperature and slow down reaction kinetics. Conversely, during hydrogen desorption, the endothermic reaction requires a continuous heat supply to sustain hydrogen release. PCM materials can act as passive thermal buffers, temporarily storing heat during absorption and releasing it during desorption. Therefore, investigating the coupled behavior of MH storage and PCM thermal management is essential to evaluate whether passive thermal buffering can effectively stabilize hydrogen release under realistic vehicle operating conditions.

Despite the recognized potential of metal hydride storage and PCM-based thermal management, their integration into vehicular applications is often addressed from different modeling perspectives depending on the target application and system scope. Several studies have investigated metal hydride-based storage for transportation systems, demonstrating its benefits in terms of energy density, safety, and thermal integration. For instance, Tribioli et al. [26] analyzed a lightweight hybrid fuel cell/battery quadricycle equipped with metal hydride storage, highlighting the performance improvements enabled by a hybrid energy storage system and effective thermal coupling between batteries and hydrides. In that work, the metal hydride tank is primarily exploited as an energy and thermal integration element within the powertrain, while the vehicle-level energy management strategy is not explicitly constrained by the dynamic hydrogen desorption behavior of the hydride storage under transient driving conditions. However, in real-world operation, where power demand fluctuations, idle phases, and thermal transients directly affect hydrogen release capability, the dynamic interaction between metal hydride behavior, thermal management, and vehicle operation becomes crucial. This underscores the need for system-level approaches that explicitly embed metal hydride storage dynamics within the vehicle simulation framework.

1.1. Contribution and objectives

The present work aims to provide a comprehensive system-level investigation of metal hydride–based hydrogen storage integrated within a fuel cell plug-in hybrid electric microcar, explicitly accounting for the coupled interactions between thermo-chemical storage dynamics, thermal management solutions, and vehicle-level operation. To the best of the authors' knowledge, this is one of the first studies to embed a physically validated metal hydride tank model, accounting for coupled heat and mass transfer, directly within a high-fidelity hybrid vehicle simulation framework, enabling real-time interaction between hydrogen desorption behavior, thermal transients, and energy management decisions. This fills a key gap in the literature, where the integration of dynamic storage constraints into control-oriented simulations of fuel cell hybrid vehicles, particularly under urban micromobility scenarios, remains largely unexplored.

To this end, an experimentally validated one-dimensional model of the metal hydride tank is embedded within a detailed hybrid vehicle simulation framework, enabling the direct coupling between hydrogen desorption behavior, FCS operation, and energy management logic. Passive thermal management approaches are investigated, including forced convection based on FCS waste heat recovery and thermal buffering through phase change materials, whose design and integration are explicitly modeled and validated. The proposed framework allows assessing not only the achievable range extension, but also hydrogen utilization effectiveness, FCS operating continuity, and system robustness under realistic driving conditions. Continuous driving cycles, sensitivity analyses, and representative urban commuting scenarios with extended parking phases are considered to capture the impact of transient operation and thermodynamic relaxation effects. By jointly analyzing storage dynamics, thermal behavior, control actions, and tank layout within a unified numerical environment, this study aims to clarify under which conditions metal hydride storage, with and without PCM-based thermal management, can represent a viable and scalable solution for sustainable micromobility applications, without relying on complex active heating systems.

2. Materials and methods

This section describes the numerical framework adopted to investigate the integration of metal hydride-based hydrogen storage into a fuel cell hybrid electric microcar. Starting from a battery-electric baseline vehicle, a hybrid architecture is developed by integrating a hydrogen-based power generation system. For clarity, a schematic overview of the resulting hybrid microcar configuration is reported in Fig. 1. The figure provides an illustrative representation of the possible volumetric integration of the main subsystems within the existing BEV architecture. It should be noted that the layout is intended only as a conceptual example.

2.1. Hybrid microcar simulation platform

The vehicle simulation platform adopted in this study builds on the numerical model previously developed by Bartolucci et al. [27], referring to a lightweight electric quadricycle manufactured by OPV Solutions S.r.l [28]. (BEV version) and used here as the baseline vehicle. Starting from the original battery-electric configuration, the architecture is extended to a fuel-cell hybrid-electric layout through the integration of a hydrogen-based auxiliary power unit, as schematically illustrated in Fig. 1.

The complete hybrid vehicle model is implemented in the MATLAB/Simulink/Simscape environment and retains the validated representation of the main powertrain components (i.e. FCS, DC/DC converter and battery pack). The traction system consists of four in-wheel electric motors, whose inverters are connected to a common DC bus that serves as the electrical interface between the propulsion system and the onboard energy sources.

The battery pack corresponds to the original BEV configuration, specifically a 16-cells air-cooled $LiFePO_4$ battery with a nominal voltage of 51.2 V and a capacity of 100 Ah, whose behavior has been experimentally characterized in Ref. [29]. The FCS subsystem is based on a commercial air-cooled Proton Exchange Membrane (PEM) fuel cell stack (Horizon H-2000, 48 cells in series, rated power $\approx$ 1.5 kW), coupled to the DC bus via a dedicated, customized DC/DC converter that accounts for voltage regulation and conversion efficiency. Details on fuel cell modeling and experimental tests can be found in Ref. [30]. For clarity, the performance curves of the PEM FCS are presented below for the Short-Circuit Unit OFF mode. Specifically, Fig. 2 (a) reports the polarization curve as function of the current (voltage range in $[28-46]$ V), compared to the power curve, which rises up to a maximum of 1.6 kW. Conversely, Fig. 2 (b) presents the efficiency characteristics of the system considered: it compares the efficiency of the stack (η_{stack}), solely related to the electrochemical conversion, to the system efficiency (η_{system}), which results from the product of η_{stack} and the hydrogen utilization factor, thus accounting for overall losses and hydrogen waste. Further details on consumption modeling and validation can be found in Ref. [27].

Power sharing between the battery and the fuel cell system is

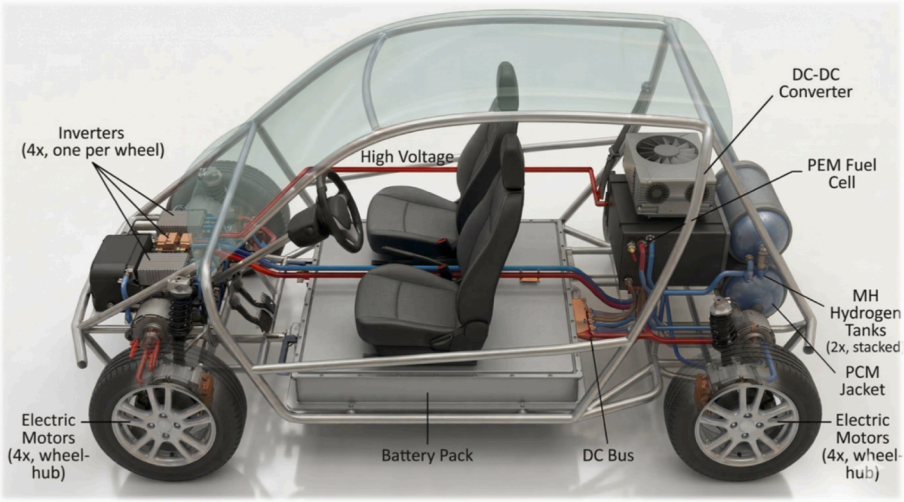

Fig. 1. Schematic layout of the fuel cell hybrid microcar architecture considered in this study. The layout is provided for illustrative purposes.

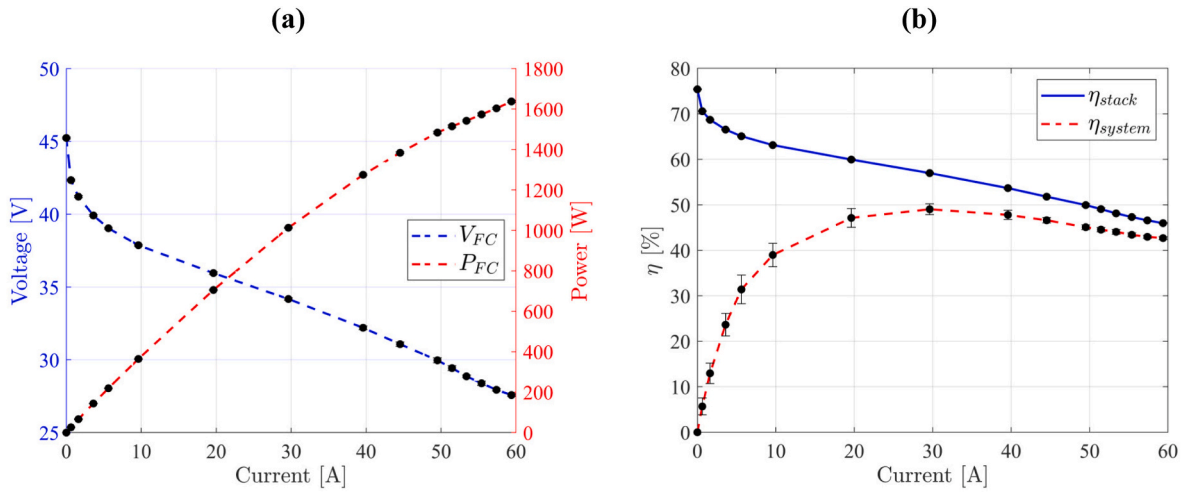

Fig. 2. Performance characteristics of the HT-PEM fuel cell stack. (a) Polarization curve and Power curve as functions of current. (b) Stack efficiency and overall system efficiency.

governed by an energy management strategy based on a range-extender architecture, which is widely adopted in the state of the art for light-weight and plug-in hybrid vehicles due to its simplicity and operational flexibility. Power allocation is performed through direct control of the DC/DC converter, based on hydrogen availability. Hydrogen supply to the FCS is provided by the metal hydride storage system, whose dynamic modeling and thermal management integration represent the main extension of the present work and are detailed in the following sections.

In the considered architecture, the fuel cell stack is not intended to continuously supply traction power, but rather operates as a range extender supporting the battery under specific operating conditions. This choice is consistent with the baseline BEV microcar configuration adopted in this study, where the battery remains the primary traction source, while the fuel cell system provides additional energy support through intermittent operation governed by the adopted energy management strategy.

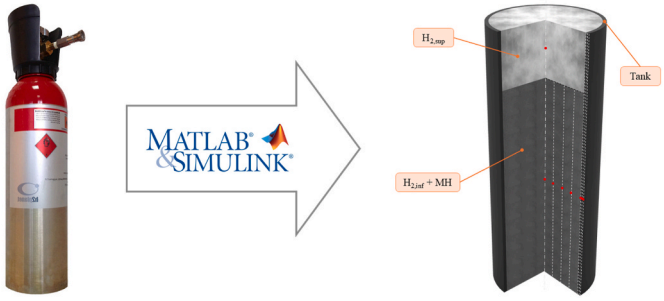

Fig. 3. One-dimensional radial discretization adopted for the metal hydride storage tank model. Red markers indicate the computational nodes used in the numerical formulation. Adapted from Ref. [31]. (For interpretation of the references to colour in this figure legend, the reader is referred to the Web version of this article.)

2.2. Metal hydrides numerical modeling

This paper examines how a detailed description of the coupled thermochemical behavior of solid-state hydrogen storage affects its integration into a vehicle-level simulation environment. The numerical model used to describe the metal hydride hydrogen storage system is directly based on the one-dimensional dynamic formulation previously developed and validated by the authors in Refs. [31], [32]. For clarity, a complete description of the governing equations, the numerical implementation, and the experimental validation is presented in the reference.

The Metal Hydride (MH) tank is modeled as an axially symmetric cylindrical domain, discretized along the radial direction (Fig. 3). A one-dimensional radial discretization is applied to the metal hydride bed, the gaseous hydrogen phase, and the tank wall, allowing the coupled solution of mass and energy conservation equations. This assumption is appropriate for cylindrical tanks with relatively high height-to-diameter ratios, for which radial thermal gradients are expected to dominate over axial ones. Also, the tank wall is treated as an additional solid domain within the radial discretization, and its thermal inertia is explicitly accounted for in the transient energy conservation equation. This formulation allows the model to capture the heat storage effect of the metallic wall and its influence on the transient thermal behavior of the hydride bed.

In the present study, the modeling framework is applied to simulate commercial metal hydride tanks filled with Hydralloy C5, supplied by H2planet (MyH2 3000 model), and integrated into the hybrid microcar simulation platform. This allows the assessment of metal hydride behavior under realistic driving conditions and its interaction with the FCS and vehicle-level control strategy.

Hydralloy C5 belongs to the AB_2 family of metal hydride alloys and is widely used in commercial hydrogen storage systems due to its favorable thermodynamic properties and good cycling stability [33]. The thermodynamic behavior of the alloy can be described through its pressure–composition–isotherm (PCI) curves, which define the relationship between hydride equilibrium pressure, temperature and hydrogen concentration in the powder. Typical PCI curves of AB_2-type alloys exhibit a characteristic plateau region associated with the coexistence between the metal and hydride phases, together with a moderate hysteresis between absorption and desorption branches. These features determine the effective operating pressure range of the storage system and therefore directly influence the hydrogen release capability during vehicle operation. Long-term experimental studies have also shown that intermetallic metal hydride systems based on AB_2-type alloys maintain stable hydrogen storage performance over extended cycling under realistic operating conditions, with limited degradation of storage capacity and good reversibility of the hydrogen sorption process [33], [34]. Representative PCI curves for Hydralloy C5 are reported in Fig. 4 to illustrate the equilibrium pressure range and hysteresis behavior of the alloy.

In order to clarify the physico-chemical properties of the adopted metal hydride material and the main geometric characteristics of the storage tank, the parameters used in the numerical model, including

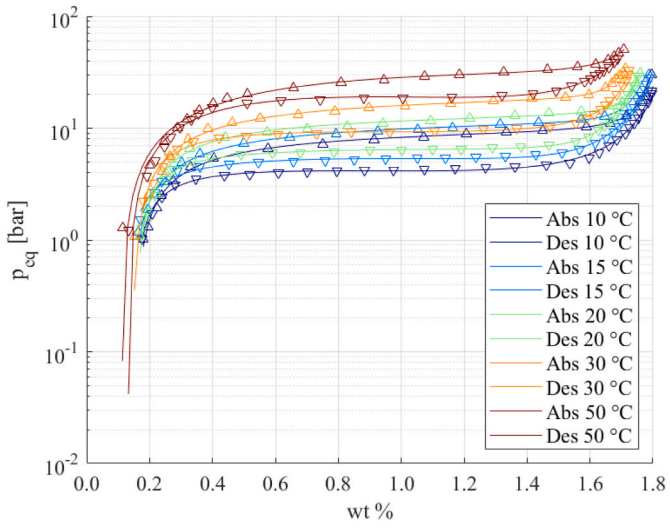

Fig. 4. Interpolated PCI curves of Hydralloy C5. Image from Ref. [31].

thermodynamic and kinetic parameters governing hydrogen sorption, are summarized in Table 1. For the validation of the PCM thermal model, a reference $LaNi_5$-based metal hydride system is considered. In contrast, the vehicle-level simulations presented in this work are based on the commercial Hydralloy C5 alloy contained in the MyH2 3000 storage tank.

2.3. PCM numerical modeling and validation

A numerical model of a configurable PCM jacket has been developed and validated in the present work. The model aims to capture the dominant thermo-physical mechanisms governing the interaction between the metal hydride tank and the surrounding PCM layer, while maintaining a level of complexity suitable for vehicle-level simulations. In particular, the formulation accounts for transient heat conduction in the PCM domain, latent heat effects associated with phase change through the enthalpy method, and radial thermal coupling with the metal hydride tank.

Table 1
Physico-chemical properties of the Hydralloy C5 metal hydride alloy and main geometric parameters of the MyH2 3000 storage tank adopted in the numerical model.

Property	Symbol	Value
Alloy composition [35]	–	Ti – Zr – Mn – V – Fe – Cr – Ni
Activation energy for desorption [36]	$E_{a,d}$	12.923 kJ mol^{-1}
Density of hydride alloy (dehydrogenated) [35]	$\rho_{MH,0}$	6300 kg m^{-3}
Density of hydride alloy (fully saturated)	$\rho_{MH,max}$	6416 kg m^{-3}
Height-to-diameter ratio	H/D	3.53
Hydride alloy type [37]		AB_2
Internal cylinder volume [37]	V_{Tank}	0.00580 m^3
Maximum H_2 charging pressure [37]		30 bar (static)
Maximum operating pressure [37]		30 bar
Maximum operating temperature [37]		65 °C
Minimum cooling temperature during charging [37]		10 °C
Molar mass of the alloy	M_{MH}	0.1037 kg mol^{-1}
Nominal capacity [37]		270 g_{H2} (≈1.6 wt%)
Occupied volume by the hydride material	V_{MH}	0.00435 m^3
Porosity	ε	0.5
Pre-exponential factor for desorption [36]	$K_{0,d}$	10.81 s^{-1}
Reaction enthalpy	ΔH_d	−27.83 kJ mol^{-1}
Reaction entropy	ΔS_d	109.90 J mol^{-1} K^{-1}
Specific heat at constant pressure [38]	$C_{p_{MH}}$	0.5 kJ kg^{-1} K^{-1}
Tank diameter [37]	D	15 cm
Tank height [37]	H	53 cm
Thermal conductivity of the metal alloy	k_{MH}	1.5 W m^{-1} K^{-1}
Thermal conductivity of the tank	k_{Tank}	55 W m^{-1} K^{-1}
Total mass of the system [37]		22 kg

Three different phase change materials are considered in the analysis: lithium nitrate trihydrate ($LiNO_3$–$3H_2O$, denoted as PCM1), the commercial salt hydrate SP29 (PCM2), and the paraffin-based material RT28HC (PCM3). The proposed PCM model is consistent with the modeling framework adopted for the metal hydride domain and is formulated using a one-dimensional radial discretization of the PCM jacket surrounding the hydride tank, capturing the dominant radial heat transfer mechanisms.

The one-dimensional radial formulation follows the approach proposed by Bartolucci and Krastev [39], who developed and validated a detailed two-dimensional CFD model of metal hydride–PCM systems in both *pool* and *jacket* configurations, considering different classes of PCMs (paraffins and salt hydrates). In the present work, axial heat transfer is neglected, which is a reasonable assumption for cylindrical tanks with high height-to-diameter ratios, where radial thermal gradients dominate over axial ones.

Moreover, buoyancy effects and natural convection within the molten PCM are not explicitly modeled, due to the inherently one-dimensional nature of the formulation. As discussed in Ref. [39], during the discharge phase of the system, corresponding to PCM solidification, the effect of buoyancy-driven convection is shown to be negligible, as natural convection is strongly suppressed in the solidifying medium. Consequently, neglecting buoyancy effects in this phase does not significantly affect the predicted thermal response of the PCM–MH system.

The governing equations adopted in the present work (Eqs. (1)–(7)) are directly derived from the formulation proposed in Ref. [39] and are reported here for completeness.

The thermal behavior of the PCM jacket is described by solving the transient energy conservation equation in cylindrical coordinates, expressed in one-dimensional radial form as:

$$\rho c_p^{eff}\frac{\partial T}{\partial t}=\frac{1}{r}\frac{\partial}{\partial r}\left(r\lambda\frac{\partial T}{\partial r}\right) \tag{1}$$

where T is the PCM temperature, λ is the effective thermal conductivity, and ρc_p^{eff} is the effective volumetric heat capacity accounting for both sensible and latent heat contributions.

Following the enthalpy method adopted in Ref. [39] and based on [40], [41], the phase-change process is modeled by introducing a liquid fraction f_L, defined as a continuous function of temperature across a finite melting interval ΔT_m centered around the melting temperature T_m. In the present implementation, f_L is defined as:

$$f_L=\begin{cases}0 & T\le T_m-\dfrac{\Delta T_m}{2}\\ \dfrac{T-\left(T_m-\dfrac{\Delta T_m}{2}\right)}{\Delta T_m} & T_m-\dfrac{\Delta T_m}{2}\le T\le T_m+\dfrac{\Delta T_m}{2}\\ 1 & T\ge T_m+\dfrac{\Delta T_m}{2}\end{cases} \tag{2}$$

The effective volumetric heat capacity is then expressed as the sum of sensible and latent contributions:

$$\rho c_p^{eff}=\rho_{avg}\left[(1-f_L)c_{p,s}+f_L c_{p,l}\right]+\rho_{avg}L_m\frac{d\gamma}{dT} \tag{3}$$

where $c_{p,s}$ and $c_{p,l}$ are the specific heats of the solid and liquid phases, respectively, L_m is the latent heat of fusion, and ρ_{avg} is the average PCM density. The term $\rho_{avg}L_m\frac{d\gamma}{dT}$ accounts for the latent heat effect during phase change.

Similarly, the effective thermal conductivity of the PCM is evaluated as a weighted average between the solid and liquid conductivities:

$$\lambda_{PCM} = (1 - f_L)\lambda_s + f_L\lambda_l \quad (4)$$

The PCM mass and volume required for a given MH application can be estimated by considering the reaction enthalpy of the metal hydrides, the total amount of hydrogen stored in the tank, and the thermophysical properties of the selected PCM. The total heat released during a complete hydrogen absorption process can be expressed as:

$$Q_{MH} = \frac{\Delta H \cdot m_{H_2}}{M_{H_2}} \quad (5)$$

where ΔH is the MH reaction enthalpy, m_{H_2} is the total mass of hydrogen absorbed by the alloy, and M_{H_2} is the molar mass of hydrogen. Assuming that this heat is entirely absorbed by the PCM through its latent heat, the required PCM mass can be estimated as:

$$m_{PCM} = \frac{Q_{MH}}{L_{m,PCM}} \quad (6)$$

and the corresponding PCM volume is obtained as:

$$V_{PCM} = \frac{m_{PCM}}{\rho_{PCM}} \quad (7)$$

where $L_{m,PCM}$, m_{PCM}, V_{PCM}, and ρ_{PCM} denote the latent heat, mass, volume, and density of the PCM, respectively.

As for the MH domain, the PCM region is discretized along the radial direction using a finite-volume formulation. For each control volume, the transient temperature evolution is obtained by balancing conductive heat fluxes at the inner and outer faces. For the outermost control volume, convective heat exchange with the external environment is also considered when applicable.

2.3.1. Model validation

The PCM model has been validated against the numerical results presented in Ref. [39] for a metal hydride–PCM system during hydrogen absorption. Three different PCMs have been considered, whose thermophysical properties are taken from reference data. The selected materials are reported in Section 2.3.

For validation purposes, a $LaNi_5$-based metal hydride alloy has been adopted, and the system geometry and initial conditions have been adapted to match those described by the authors. Specifically, an initial uniform temperature of 293 K has been imposed throughout system. A hydrogen charging pressure of 8 bar has been applied. In accordance with the reference study, the separating wall between the metal hydride bed and the PCM jacket has been removed, allowing direct conductive heat exchange between the two domains.

The comparison focuses on key quantities such as hydrogen absorption dynamics and f_L evolution over time. The results, reported in Fig. 5, show very good agreement between the proposed model and the reference data for all three PCMs, with relative deviations consistently below 10%. These results confirm that the simplified one-dimensional PCM formulation can accurately reproduce the thermal behavior of the MH–PCM system during phase change, while retaining a computational efficiency suitable for vehicle-level simulations.

2.4. Coupling between metal hydride storage and vehicle powertrain architecture

In the present work, a Fuel Cell Plug-in Hybrid Electric Vehicle (FCPHEV) architecture is adopted, in which the battery pack is the primary traction source. In this configuration, the FCS is not intended to continuously supply traction power, but rather to act as an auxiliary energy source that supports the battery under specific operating conditions. This architecture is adopted because fuel cell systems typically exhibit slower dynamic response compared to electrochemical batteries and are therefore less suitable for following rapid power transients associated with vehicle traction. Consequently, the battery pack acts as the primary energy buffer for propulsion and regenerative braking, while the FCS operates at nearly constant power to recharge the battery and extend the vehicle driving range.

Furthermore, MH storage dynamics are explicitly integrated into the vehicle control strategy via a pressure-based thermostatic controller. FCS activation and deactivation are governed by the comparison between the MH tank pressure and the FCS operating pressure, ensuring hydrogen availability while preventing critical operating conditions of the storage system.

3. Results and discussion

To evaluate system behavior under representative driving conditions, the vehicle was simulated over consecutive World Motorcycle Test Cycles (WMTC), considering only the urban phase of the cycle. This choice reflects the microcar's operational constraints, with a maximum speed of 45 km/h, making the urban segment fully representative of its intended use. Each WMTC corresponds to approximately 3.5 km of driving distance.

The MH storage system consists of a Hydralloy C5-based tank with an internal volume of 5.8 L (H2 Planet, MyH2 3000), capable of storing up to 270 g of hydrogen per unit. Different thermal management solutions

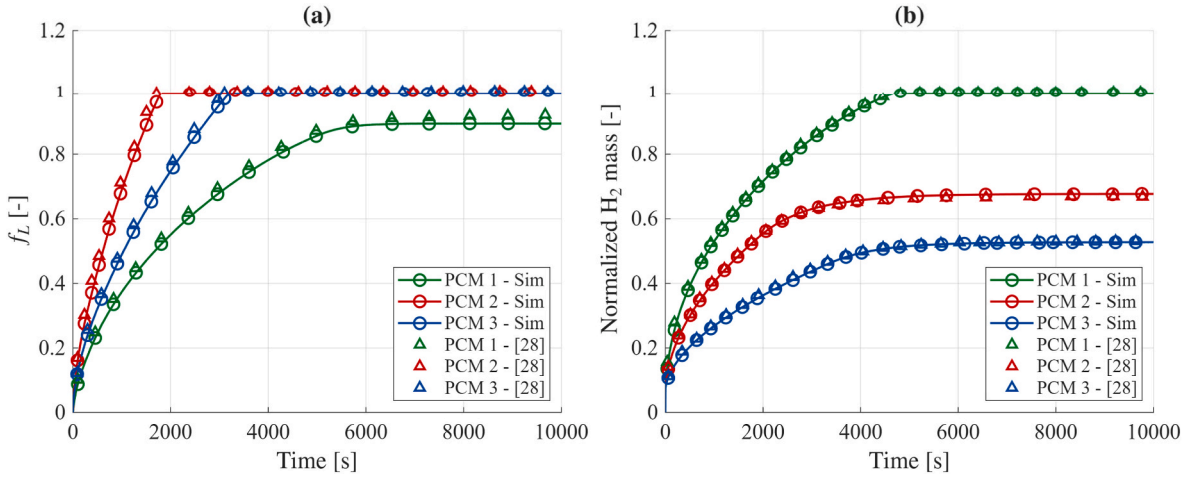

Fig. 5. Validation of the PCM numerical model against reference data during hydrogen absorption. (a) Time evolution of the f_L for the metal hydride system thermally coupled with different PCMs. (b) Corresponding evolution of the normalized absorbed hydrogen mass. Solid lines represent simulation results while markers indicate reference data from the literature.

are investigated in the following to identify the optimal trade-off among thermal effectiveness, system complexity, and overall performance. Emphasis is placed on each solution's ability to maintain the MH bed under favorable thermal conditions, ensuring sustained hydrogen desorption compatible with the FCS demand.

Two main thermal management strategies are considered. The first one is based on forced convection, achieved by directing the warm exhaust air from the FCS blowers toward the MH canisters. The exhaust air temperature under steady operation of the fuel cell system at 1.5 kW is approximately 50 °C. The second strategy relies on integrating Phase Change Materials (PCMs) to passively buffer the thermal effects associated with hydrogen absorption and desorption.

Regarding PCM integration, a jacket configuration is analyzed consistently with the one-dimensional nature of the developed numerical model. A salt hydrate PCM is considered, namely PCM1 introduced in the previous section. The required PCM quantity is determined by applying Eqs. (12)–(14), leading to a total PCM volume of $7.7 \cdot 10^{-3}$ m^3 and an overall PCM mass of approximately 16 kg. The jacket height is fixed and equal to the MH tank height, while the resulting thickness is derived from the computed PCM volume.

Concerning the EMS, as reported in Section 2.1, a Range Extender (RE) strategy is implemented into the vehicle platform. In this configuration, the FCS is operated as an auxiliary power unit, with the primary objective of extending the vehicle range. Therefore, the FCS operates at nearly constant power (rated power) of 1.5 kW, with the duty cycle only controlled by the MH pressure-based thermostatic controller.

All simulations assume MH tanks initially fully charged with hydrogen. The ambient temperature is set to 25 °C, which also corresponds to the initial temperature of the MH bed when no PCM jacket is present. Conversely, when a PCM jacket is included, the initial temperature of the coupled MH–PCM system is set to 35 °C, to ensure that the PCM is fully in the liquid phase at the beginning of the simulation and therefore able to provide its maximum latent heat buffering capability. This condition represents a preliminary warm-up of the PCM jacket, which can be achieved through auxiliary heating integrated into the storage system. Such heating may be supplied either during vehicle charging phases in a plug-in configuration, or, if required, by drawing a limited amount of energy from the battery pack, resulting in a controlled and temporary reduction of the available electrical energy for traction. The energy required for this preliminary thermal conditioning is not explicitly included in the vehicle energy balance, since the objective of this work is to investigate the thermo-chemical interaction between metal hydride storage, thermal management strategies, and vehicle operation. In addition, the heat released during hydrogen refueling naturally increases the MH temperature and can be partially absorbed by the PCM, facilitating its liquefaction prior to the subsequent discharge phase. The initial equilibrium pressure of the MH bed is consistently determined from the initial temperature.

All simulations are carried out assuming an initial battery SOC equal to 70%. This value is deliberately set below the threshold required to enable full regenerative braking, due to the presence of a SOC-based regenerative braking logic implemented in the vehicle model, thereby ensuring consistent comparison and reliable extrapolation of vehicle performance across all simulated configurations.

Each simulation is stopped when the battery SOC reaches 10%, regardless of the amount of hydrogen remaining in the metal hydride tank. This criterion ensures a consistent definition of vehicle range across all configurations, while allowing the effective utilization of hydrogen storage to be evaluated separately.

System performance is evaluated through a set of Key Performance Indicators (KPIs), reported in Table 2, specifically selected to capture the interaction between FCS operation, hydrogen availability and MH thermal behavior.

A preliminary comparison is conducted to provide an initial overview of the achievable benefits of the proposed thermal management strategies relative to the original BEV configuration. In this analysis, a range extender control strategy is adopted for the hybrid configurations, and a single MH tank is installed in the rear section of the microcar. The results, reported in Fig. 6, compare the achievable vehicle range and the corresponding FCS energy share for three configurations: the reference BEV, the FCPHEV with forced-convection-based thermal management (FC), and the FCPHEV equipped with PCM-based thermal management (PCM).

Table 2
Key Performance Indicators (KPIs) adopted for system performance assessment.

KPI	Unit	Name	Description
EC_{FCS}	kWh	FCS Energy Contribution	Net electrical energy delivered by the FCS system over the entire simulation.
EC_{BESS}	kWh	BESS Energy Contribution	Net electrical energy delivered by the battery over the full mission.
ec_{FCS}	kWh/km	FCS Specific Energy Contribution	FCS energy contribution normalized by the total driven distance.
DC_{FCS}		FCS Duty Cycle	Ratio between the FCS operating time and the total simulation time.
FC_{SI}	kg^{-1}km^{-1}	FCS Specific Idling	Indicator of FCS idling events due to insufficient hydrogen supply normalized both by the total driven distance and the total consumed hydrogen.
$H_{2,frac}$		Utilized Hydrogen Fraction	Ratio between the hydrogen consumed by the FCS and the hydrogen initially stored.
ES_{FCS}		FCS Energy Share	Fraction of total vehicle energy demand supplied by the FCS system.
e_{EM}	kWh km^{-1}	Electric Motor Specific Energy	Electric energy consumed by the traction motor per unit distance traveled.
u_{H_2}	km kg^{-1}	Hydrogen Utilization Indicator	Additional vehicle range enabled by the FCS per unit mass of hydrogen loaded in the MH system.

The results show that forced convection increases vehicle range by approximately 40% compared to the BEV configuration. However, this improvement is associated with a relatively low FCS energy share, indicating limited and discontinuous FCS utilization, likely due to sub-optimal thermal conditions in the MH tank. In contrast, adopting PCM-based thermal management further increases vehicle range to nearly 120 km, representing an additional improvement of approximately 35%

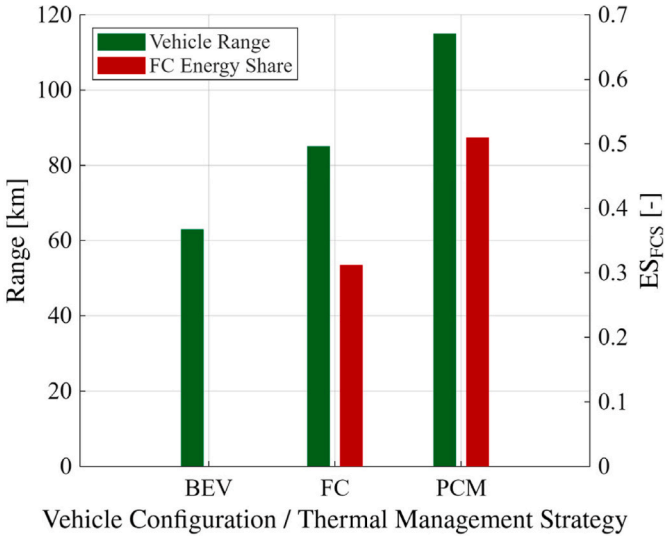

Fig. 6. Vehicle range and FCS energy share for the reference BEV configuration and FCPHEV layouts with forced-convection-based and PCM-based thermal management, considering a single metal hydride tank and a range-extender control strategy.

compared to the forced convection case. More importantly, this configuration achieves an FCS energy share close to 50%, highlighting a substantially improved exploitation of the FCS and a more effective hydrogen release from the MH storage system.

This improvement is primarily related to the thermal buffering capability of the PCM jacket. During the desorption phase, stored thermal energy in PCMs can be gradually released, helping to sustain the endothermic hydrogen desorption process. As a result, the MH bed temperature remains closer to the equilibrium conditions required for hydrogen release, preventing premature pressure drops in the tank and avoiding frequent shutdowns of the FCS due to insufficient hydrogen supply.

This result highlights that, in MH-based storage systems for vehicular applications, thermal management and tank configuration play a dominant role in determining vehicle-level performance. In fact, hydrogen desorption is strongly temperature-dependent, and insufficient heat supply rapidly reduces the equilibrium pressure of the hydride bed, limiting hydrogen availability to the FCS and therefore its effective contribution to propulsion.

3.1. Thermal management and tank layout

The specific impact of the thermal management strategy and the metal hydride tank layout on the achievable vehicle performance is investigated in the present section. As a reference baseline, the original battery electric vehicle configuration achieves a driving range of approximately 65 km, considering a battery discharge window from 70% to 10% SOC.

The first comparison, reported in Fig. 7(a), focuses on the effect of different thermal management strategies—namely Natural Convection (NC), Forced Convection (FC), and PCM jacket—considering a single MH tank configuration. Both the achievable vehicle range and the FCS idling indicator are reported. As expected, natural convection cannot sustain the hydrogen desorption rates required by the FCS. Therefore, the system rapidly reaches critical operating conditions that trigger frequent FCS idling events, without a sufficient recovery capacity to guarantee continuous operation. This behavior results in a limited vehicle range (similar to that of a BEV) and confirms the inadequacy of natural convection for on-board MH-based hydrogen storage.

The adoption of forced convection improves system performance by enhancing heat transfer at the MH tank boundary, allowing a partial stabilization of the desorption process. This translates into an increased vehicle range and a reduction in FC_{SI} compared to the natural convection case.

The integration of a PCM jacket significantly improves system behavior. For the single-tank configuration, PCM-based thermal management leads to the highest achievable range among the investigated strategies and to a marked reduction in FC_{SI}. This improvement can be directly linked to the thermal buffering capability of the PCM, as illustrated in Fig. 7(c), where the temperature evolution of the inner and outer MH nodes is compared with that of the PCM nodes. While the MH bed experiences significant temperature drops during hydrogen

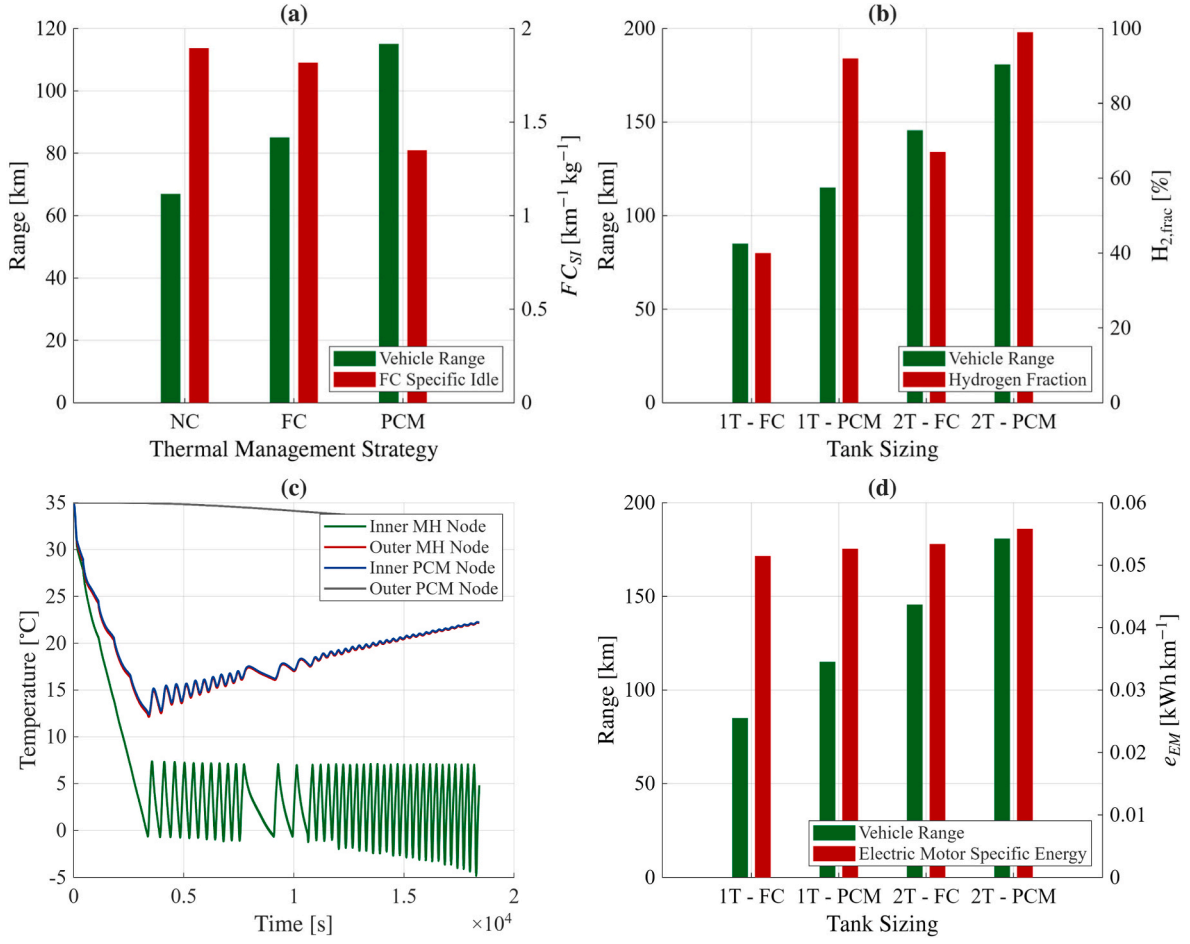

Fig. 7. Impact of thermal management strategy and metal hydride tank layout on vehicle performance under range extender control: (a) vehicle range and FCS idling frequency for different thermal management strategies with a single MH tank; (b) vehicle range and hydrogen utilization for single- and dual-tank configurations; (c) temperature evolution of inner and outer MH and PCM nodes for the PCM-based case; (d) vehicle range and specific electric motor energy for single- and dual-tank configurations.

desorption, the PCM maintains a smoother thermal profile, owing to its phase change, and effectively damps temperature oscillations at the MH–PCM interface, keeping the MH bed closer to favorable operating conditions.

During vehicle operation, PCM progressively releases latent heat, leading to a gradual decrease of f_L, whose average value approaches 60% at the end of the simulation. This effect helps to sustain hydrogen desorption without requiring active thermal control, enabling more continuous FCS operation and explaining the reduced idling frequency observed in the PCM case.

To further improve vehicle range, a dual-tank configuration is subsequently analyzed, as reported in Fig. 7(b). In this case, vehicle performance is influenced not only by increased hydrogen availability but also by the additional mass burden introduced by the second MH tank and, when applicable, by the corresponding PCM jacket. The added mass amounts to approximately 25 kg for an additional MH tank and about 16 kg for an additional PCM jacket.

A key effect of adopting two MH tanks in parallel is the relaxation of the desorption process in each individual tank, due to the halved hydrogen mass flow rate required per tank. This effect is particularly evident in the forced convection case, where $H_{2,frac}$ increases from approximately 40% in the single-tank configuration (about 110 g of hydrogen) to around 68% in the dual-tank configuration (approximately 370 g). As a result, the dual-tank layout enables a significantly more stable FCS operation, making forced convection a viable option when multiple MH tanks are employed.

To separate the effect of the increased hydrogen storage capacity from the improvements in the vehicle hydrogen utilization, Table 3 compares the Hydrogen Utilization Indicator, u_{H_2}, across the different configurations, where ΔR denotes the additional driving range enabled by the FCS relative to the original BEV architecture.

Using the forced-convection single-tank case as a reference, if the range extension were solely due to the doubled hydrogen storage, the expected ΔR for the dual-tank configuration would scale linearly with hydrogen utilization, yielding an estimated value of approximately 44 km. In contrast, the simulated vehicle achieves a ΔR of 83 km, clearly demonstrating that the observed performance gain cannot be attributed to storage capacity alone.

Consistently, the Hydrogen Utilization Indicator u_{H_2} increases by 86%, rising from 82 km kg^{-1} to 153 km kg^{-1}. This substantial improvement indicates a more effective thermodynamic exploitation of the stored hydrogen in the dual-tank configuration. By reducing the hydrogen desorption load per tank, temperature drops within the metal hydride bed are mitigated, equilibrium conditions are maintained closer to their optimal range, and fuel-cell idling events are significantly reduced.

Conversely, PCM-based thermal management consistently guarantees high hydrogen utilization and stable FCS operation, regardless of the number of tanks. In the dual-tank PCM configuration, the combined effects of enhanced thermal buffering and reduced per-tank desorption load lead to the best overall performance. In this scenario, the microcar achieves a driving range of approximately 180 km, nearly three times that of the original BEV configuration.

From a system design perspective, these results highlight a clear trade-off between increased vehicle mass and achievable performance gains. Although the integration of MH tanks and PCM jackets increases the overall vehicle mass compared to the baseline BEV configuration, the additional energy supplied by hydrogen largely compensates for this penalty, resulting in a net improvement in driving range. The additional mass associated with extra MH tanks and PCM jackets leads to a e_{EM} increase, as shown in Fig. 7(d). This penalty becomes more pronounced when moving from a single-to a dual-tank configuration and when integrating PCM jackets. However, despite the increase in e_{EM}, the achievable driving range increases monotonically across all configurations. This behavior indicates that the benefits associated with enhanced thermal buffering and reduced per-tank hydrogen desorption load largely outweigh the mass-induced efficiency penalty. In particular, the combination of PCM-based thermal management and multiple MH tanks emerges as the favorable choice, enabling substantial range extension while preserving stable FCS operation and high hydrogen utilization.

Table 3
Additional range and hydrogen utilization indicator for different thermal management strategies and tank layouts.

Thermal Management	Tanks No.	ΔR	u_{H_2}
Forced Convection	1	22 km	82 km kg^{-1}
	2	83 km	153 km kg^{-1}
PCM	1	52 km	193 km kg^{-1}
	2	118 km	218 km kg^{-1}

3.2. Pressure threshold sensitivity analysis

A key element of the proposed control strategy is the FCS activation pressure threshold, which defines the metal hydride tank pressure at which the FCS is allowed to switch on. In all simulated configurations, the FCS is turned off when the pressure inside the metal hydride tanks decreases to 2.5 bar, while the activation threshold is varied to investigate its influence on overall system behavior. To this end, a set of simulations is performed by varying the FCS turn-on pressure between 3.0 and 5.0 bar.

The resulting impact on vehicle performance is reported in Fig. 8(a), where the achievable driving range is shown for both forced-convection-based and PCM-based thermal management strategies. When forced convection is used, the activation pressure threshold clearly influences vehicle range: increasing the threshold results in a progressive reduction in achievable range. The best performance is obtained at an activation pressure of 3.0–3.5 bar, for which the vehicle range is approximately 1.8 times that of the original battery-electric configuration. Conversely, higher activation thresholds result in a noticeable performance degradation, with a reduction of about 5-8% in the achievable range between the optimal and worst configurations.

A significantly different trend is observed when a PCM-based thermal management strategy is employed. In this case, the achievable vehicle range remains nearly constant over the entire investigated range of activation pressures. This indicates that the thermal buffering provided by the PCM jacket stabilizes the temperature of the metal hydride bed, allowing hydrogen desorption to be sustained even at higher pressure thresholds, and therefore mitigating the negative impact of conservative activation settings.

The underlying mechanisms behind these trends are further clarified by the pressure time histories reported in Fig. 8(b), which refer to the forced-convection case for two representative activation thresholds (3.0 bar and 5.0 bar). For the sake of clarity, only the first 10000s-stretch of the simulations are reported to underline pressure behavior. At lower activation pressure, the pressure signal exhibits relatively frequent oscillations within the operating window, enabling a longer cumulative hydrogen supply while increasing the FCS starts and stops. In contrast, at higher activation pressures, the pressure evolution exhibits wider excursions and longer recovery phases between successive FCS activations. This behavior reflects slower desorption dynamics and a reduced ability of the MH system to restore favorable pressure conditions after each shutdown; however, the FCS experiences fewer start and stop events than in the previous case.

Overall, these results confirm that PCM integration improves the effective coupling between metal hydride storage and FCS operation. By reducing the sensitivity of hydrogen desorption to pressure threshold selection, PCMs enhance vehicle range and increase the robustness of the control strategy, relaxing tuning requirements while preserving stable system behavior.

Regarding system design, a trade-off is therefore crucial, with the aim of prolonging hydrogen supply and mitigating the FCS

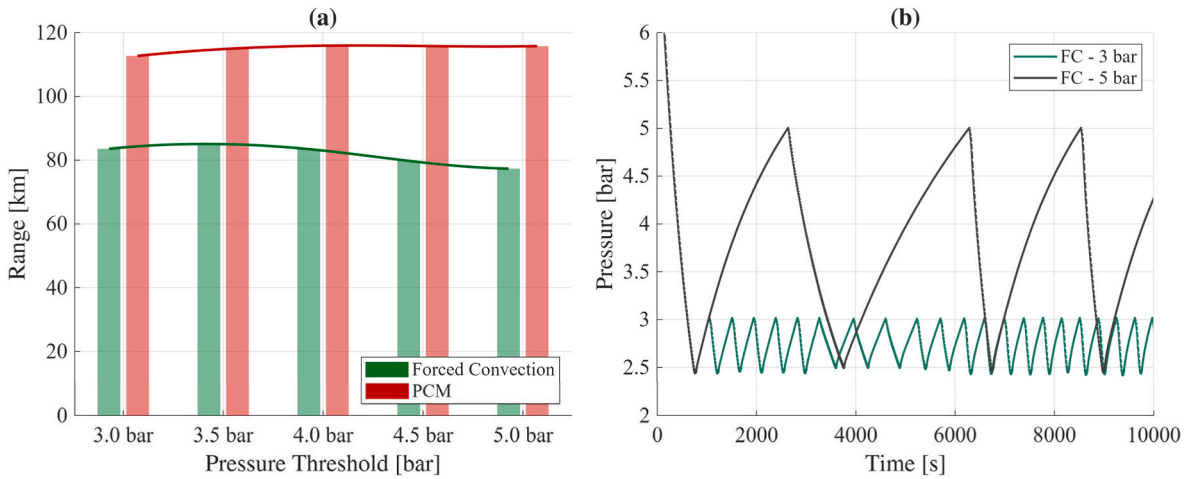

Fig. 8. Influence of FCS activation pressure threshold on system behavior: (a) vehicle range for forced-convection-based and PCM-based thermal management strategies; (b) metal hydride pressure evolution for different activation thresholds.

deactivations. From a forced-convection perspective, lower pressure thresholds significantly enhance vehicle performance, and the design should focus on maximizing the available driving range. Conversely, when adopting PCM-based thermal management strategy, higher pressure thresholds can help prevent frequent FCS start-stop cycles, as their impact on overall hydrogen fueling system stability is less pronounced.

3.3. Real life driving scenario

Up to this point, system performance has been evaluated by concatenating multiple WMTC driving cycles, thus emulating continuous vehicle operation until battery depletion. While this approach is useful to assess the maximum achievable range under sustained driving conditions, it does not fully reflect the typical usage profile of a light-weight urban vehicle, which is more likely to operate over short daily distances mixed with prolonged parking periods.

For this reason, a final set of simulations is performed to emulate a more realistic urban driving scenario. In this framework, the vehicle is operated for 20 km, assumed as an average home-to-work commuting distance, followed by an 8-h parking period representative of working time. The same pattern is then repeated for the return trip, followed by an additional 8-h parking period, i.e. overnight. This daily cycle is iterated until the vehicle can no longer complete the prescribed driving distance.

The objective of this analysis is to assess whether prolonged resting periods can promote a partial relaxation of the metal hydride thermodynamic state, thereby enhancing hydrogen desorption capability and extending vehicle range even in the absence of dedicated thermal management systems such as PCM jackets. Accordingly, the simulations are performed assuming forced convection thermal management during driving phases, when the FCS is active, and natural convection during parking periods, when the FCS is switched off. Two configurations are considered to evaluate the effect of tank layout, namely a single-tank and a dual-tank metal hydride layout.

Unlike previous analyses, the initial battery SOC is set to 100% for these simulations to better reflect real-life usage conditions, where the vehicle is typically charged overnight.

The results are reported in Fig. 9. The left panel shows the temporal evolution of the battery State of Charge for both configurations, characterized by a stepwise decrease associated with successive commuting cycles. In the single-tank configuration, and in the absence of intermediate battery recharging or hydrogen refilling, the vehicle can operate for approximately two and a half days, corresponding to a total driven distance of about 140 km. In this case, approximately 79% of the hydrogen stored in the metal hydride tank is effectively utilized, corresponding to about 213 g out of the 270 g available.

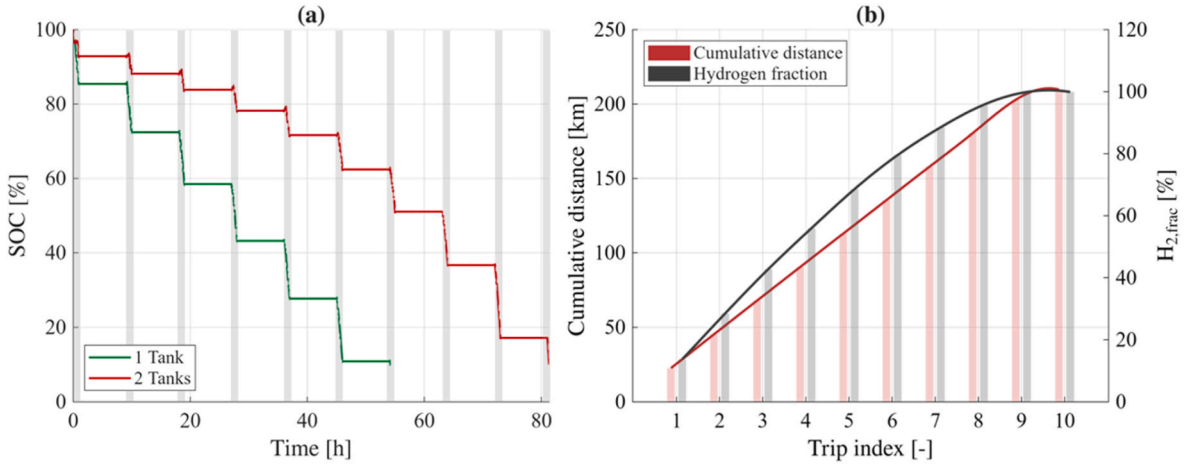

Fig. 9. (a) Battery SOC evolution during consecutive urban commuting cycles with driving (gray bars) and parking (blank) phases, comparing single- and dual-metal-hydride-tank configurations under range extender control. (b) Cumulative driven distance and corresponding hydrogen consumption as a function of trip index for the dual-tank configuration.

When two metal hydride tanks are installed in parallel, the relaxation of the desorption process in each individual tank leads to a more stable hydrogen supply to the FCS, as previously demonstrated, and a further extension of vehicle operating time. Under the same operating assumptions, the dual-tank configuration allows operation for roughly three and a half days, yielding a total driven distance of approximately 210 km. In this case, hydrogen utilization increases to approximately 99% of the total available storage, corresponding to about 535 g out of 540 g. These results confirm that parallel tank layout significantly improves hydrogen exploitation, even in realistic stop-and-go usage patterns characterized by long parking periods.

Additional insight is provided by the right panel of Fig. 9, which refers exclusively to the dual-tank configuration. The figure reports the cumulative driven distance and $H_{2,frac}$ as a function of the trip index. The smooth and progressive depletion of the hydrogen resource over successive trips confirms that the combined effect of increased storage capacity and intermittent operation enables an efficient and sustained exploitation of the metal hydride system. Notably, hydrogen consumption remains well distributed across the commuting cycles, indicating that the resting periods are effective in restoring favorable desorption conditions without inducing abrupt depletion or premature FCS shutdowns.

It is worth noting that, in a real-world scenario, the achievable range could be further extended by considering periodic battery recharging during parking phases or partial hydrogen refilling of the metal hydride tanks, possibly accompanied by controlled thermal conditioning. Therefore, the present analysis should be regarded as a conservative assessment, highlighting the intrinsic benefits of metal hydride storage and tank layout under realistic urban operating conditions.

4. Conclusions

This work investigated the integration of metal hydride–based hydrogen storage within a fuel cell plug-in hybrid electric microcar, focusing on the interplay between storage thermo-chemical dynamics, passive thermal management solutions, and vehicle-level operation under realistic urban conditions. By embedding a validated one-dimensional metal hydride model into a hybrid vehicle simulation framework, the study enabled a consistent assessment of hydrogen availability, FCS operation, and vehicle performance within an architecture representative of lightweight and plug-in micromobility applications.

The main outcomes of the analysis can be summarized as follows:

- Natural convection has been proven to be unsuitable to sustain the hydrogen desorption rates required by the FCS, resulting in frequent idling events and limited hydrogen utilization. Forced convection based on FCS waste heat recovery provides a first improvement, enabling a vehicle range increase of about 40% compared to the BEV baseline. The introduction of PCMs as passive thermal buffers leads to a substantial change in system behavior. Latent heat storage stabilizes the MH temperature during desorption, significantly reducing FCS idlings and increasing hydrogen utilization beyond 90% in single-tank configuration. As a result, FCS operation becomes more continuous, and ES_{FCS} approaches 50%, indicating a markedly improved balance between battery and FCS contributions within the hybrid powertrain.
- Increasing the number of MH tanks further relaxes desorption constraints by lowering the required hydrogen mass flow rate per tank. In forced-convection configurations, this translates into an increase in DC_{FCS} from 34 % to nearly 65 %. When combined with PCM-based thermal management, the dual-tank layout enables almost complete exploitation of the onboard hydrogen availability, with driving ranges scoring 180 km, nearly three times that of the original BEV configuration. Despite the additional mass associated with extra tanks and PCM jackets, the resulting efficiency penalty is outweighed by the gains in hydrogen availability and operational continuity.
- Concerning the sensitivity to FCS activation pressure, activation pressures ranging from 3.0 to 5.0 bar lead to a reduction in achievable range of about 5–8% for FC configurations. Conversely, PCM-based configurations exhibit a nearly invariant vehicle range over the same pressure interval.
- When moving from continuous driving cycles to a realistic urban usage pattern characterized by alternating driving and parking phases, MH systems further benefit from thermodynamic relaxation during rest periods. Under these conditions, hydrogen utilization reaches approximately 79% in single-tank configurations and up to 99% with two tanks, enabling multi-day vehicle operation also for FC thermal management, without intermediate recharging or hydrogen refilling.

Overall, the results indicate that, when supported by passive PCM-based thermal management and suitable tank integration, MH–based hydrogen storage can reliably sustain FCS operation in a hybrid architecture tailored for urban micromobility. By effectively overcoming the thermal constraints that have traditionally hindered metal hydride deployment in mobile applications, the proposed approach contributes to reducing the main barriers to the implementation of solid-state hydrogen storage systems, shifting metal hydride storage from a limiting factor to an enabling technology for lightweight, plug-in fuel cell hybrid vehicles, while preserving their inherent advantages in terms of low-pressure operation, safety, renewable-friendliness and cost-effectiveness.

CRediT authorship contribution statement

L. Bartolucci: Writing – review & editing, Supervision, Project administration, Methodology, Funding acquisition, Conceptualization. **E. Cennamo:** Writing – review & editing, Supervision, Software, Methodology, Conceptualization. **S. Cordiner:** Writing – review & editing, Supervision, Project administration, Funding acquisition, Conceptualization. **V.K. Krastev:** Writing – review & editing, Supervision, Methodology, Conceptualization. **V. Mulone:** Writing – review & editing, Supervision, Project administration, Funding acquisition, Conceptualization. **A. Polimeni:** Writing – original draft, Visualization, Validation, Software, Methodology, Investigation, Formal analysis, Data curation, Conceptualization.

Declaration of generative AI in the manuscript preparation process

During the preparation of this work, the authors used ChatGPT and Claude solely for language editing and stylistic refinement of the manuscript. The scientific content, data analysis, modeling, interpretation of results, and conclusions were entirely conceived and developed by the authors. After using these tools, the authors carefully reviewed and edited the text and took full responsibility for the content of the published article.

Declaration of competing interest

The authors declare that they have no known competing financial interests or personal relationships that could have appeared to influence the work reported in this paper.

Acknowledgements

The authors acknowledge partial support from the National Center for HPC, Big Data and Quantum Computing, Project CN_00000013 - CUP: E83C22003230001, Mission 4 Component 2 Investment 1.4, funded by the European Union - Next Generation EU.

References

[1] Sang Y, Zhang Z, Liu S, Song C. Decarbonization pathways in the transport sector: a review of integrated assessment models and future directions for model improvement. Renew Sustain Energy Rev Jan. 2026;225:116204. https://doi.org/10.1016/j.rser.2025.116204.

[2] Matura A, Singh RK, Kumar R. Decarbonizing road transport: a systematic literature review based on use case analysis. Case Studies on Transport Policy Jun. 2025;20:101416. https://doi.org/10.1016/j.cstp.2025.101416.

[3] Mavlutova I, Atstaja D, Grasis J, Kuzmina J, Uvarova I, Roga D. Urban transportation concept and sustainable urban mobility in smart cities: a review. Energies Apr. 2023;16(8):3585. https://doi.org/10.3390/en16083585.

[4] Winkler L, Pearce D, Nelson J, Babacan O. The effect of sustainable mobility transition policies on cumulative urban transport emissions and energy demand. Nat Commun Apr. 2023;14(1):2357. https://doi.org/10.1038/s41467-023-37728-x.

[5] Shang W-L, et al. Congestion and pollutant emission analysis of urban road networks based on floating vehicle data. Urban Clim Jan. 2024;53:101794. https://doi.org/10.1016/j.uclim.2023.101794.

[6] Chen Y, Li C, Wang W, Zhang Y, Chen XM, Gao Z. The landscape, trends, challenges, and opportunities of sustainable mobility and transport. npj Sustain Mobil Transp Feb. 2025;2(1):8. https://doi.org/10.1038/s44333-025-00026-8.

[7] Homem De Almeida Rodriguez Correia G. Increasing transport sustainability through the integration between power grids and electric mobility systems. npj Sustain Mobil Transp Apr. 2025;2(1):17. https://doi.org/10.1038/s44333-025-00036-6. s44333-025-00036–6.

[8] Yan W, et al. Assessing the environmental benefits of passenger cars electrification in metropolises: a case study of Singapore. Int J Sustain Transp Aug. 2025;19(8):749–61. https://doi.org/10.1080/15568318.2024.2421840.

[9] Bartolucci L, Cennamo E, Cordiner S, Mulone V, Pasqualini F, Boot MA. Digital twin of a hydrogen fuel cell hybrid electric vehicle: effect of the control strategy on energy efficiency. Int J Hydrogen Energy Jun. 2023;48(54):20971–85. https://doi.org/10.1016/j.ijhydene.2022.11.283.

[10] Günaydın ÖF, Topçu S, Aksoy A. Hydrogen fuel cell vehicles: overview and current status of hydrogen mobility. Int J Hydrogen Energy Jun. 2025;142:918–36. https://doi.org/10.1016/j.ijhydene.2025.01.412.

[11] Le TT, et al. Fueling the future: a comprehensive review of hydrogen energy systems and their challenges. Int J Hydrogen Energy Feb. 2024;54:791–816. https://doi.org/10.1016/j.ijhydene.2023.08.044.

[12] Togun H, et al. A review on recent advances on improving fuel economy and performance of a fuel cell hybrid electric vehicle. Int J Hydrogen Energy Nov. 2024;89:22–47. https://doi.org/10.1016/j.ijhydene.2024.09.298.

[13] Khalatbarisoltani A, Zhou H, Tang X, Kandidayeni M, Boulon L, Hu X. Energy management strategies for fuel cell vehicles: a comprehensive review of the latest progress in modeling, strategies, and future prospects. IEEE Trans Intell Transport Syst Jan. 2024;25(1):14–32. https://doi.org/10.1109/TITS.2023.3309052.

[14] Bartolucci L, Cennamo E, Cordiner S, Donnini M, Grattarola F, Mulone V. Fuel cell hybrid electric vehicle: an integrated approach for sub-optimal controller in real-time application. SAE Int J Adv & Curr Prac in Mobility Apr. 2024;7(2):683–92. https://doi.org/10.4271/2024-01-2187.

[15] Schlapbach L, Züttel A. Hydrogen-storage materials for mobile applications. Nature 2001;414(Nov).

[16] Scarpati G, Frasci E, Di Ilio G, Jannelli E. A comprehensive review on metal hydrides-based hydrogen storage systems for mobile applications. J Energy Storage Nov. 2024;102:113934. https://doi.org/10.1016/j.est.2024.113934.

[17] Hasnain M, Sezer H, Mason JH. Modeling heat and mass transfer in metal hydride hydrogen storage systems: impact of operating parameters and reactor geometry. Int J Hydrogen Energy Jun. 2024;71:1045–55. https://doi.org/10.1016/j.ijhydene.2024.05.311.

[18] Chung CA, Ho C-J. Thermal–fluid behavior of the hydriding and dehydriding processes in a metal hydride hydrogen storage canister. Int J Hydrogen Energy May 2009;34(10):4351–64. https://doi.org/10.1016/j.ijhydene.2009.03.028.

[19] Nguyen HQ, Shabani B. Metal hydride thermal management using phase change material in the context of a standalone solar-hydrogen system. Energy Convers Manag Nov. 2020;224:113352. https://doi.org/10.1016/j.enconman.2020.113352.

[20] Drawer C, Lange J, Kaltschmitt M. Metal hydrides for hydrogen storage – identification and evaluation of stationary and transportation applications. J Energy Storage Jan. 2024;77:109988. https://doi.org/10.1016/j.est.2023.109988.

[21] Nyamsi SN, Tolj I. The impact of active and passive thermal management on the energy storage efficiency of metal hydride pairs based heat storage. Energies May 2021;14(11):3006. https://doi.org/10.3390/en14113006.

[22] Nyamsi SN, Tolj I. Metal hydride reactors and phase change materials: enhancing energy storage for medium-high power vehicles. J Energy Storage Dec. 2024;104:114545. https://doi.org/10.1016/j.est.2024.114545.

[23] Xu Y, McCurdy M, Farid M. The use of phase change materials for thermal management of metal hydride reaction. Appl Sci Sep. 2025;15(17):9657. https://doi.org/10.3390/app15179657.

[24] Yao J, et al. A continuous hydrogen absorption/desorption model for metal hydride reactor coupled with PCM as heat management and its application in the fuel cell power system. Int J Hydrogen Energy Oct. 2020;45(52):28087–99. https://doi.org/10.1016/j.ijhydene.2020.05.089.

[25] El Mghari H, Huot J, Tong L, Xiao J. Selection of phase change materials, metal foams and geometries for improving metal hydride performance. Int J Hydrogen Energy May 2020;45(29):14922–39. https://doi.org/10.1016/j.ijhydene.2020.03.226.

[26] Tribioli L, Di Ilio G, Jannelli E. Fuel cell/battery hybrid lightweight quadricycle with metal hydride hydrogen storage for improved performance. In: Presented at the 16th International Conference on Engines & Vehicles, Capri, Italy; Aug. 2023. https://doi.org/10.4271/2023-24-0137. 2023-24–0137.

[27] Bartolucci L, Cennamo E, Cordiner S, Donnini M, Mulone V. Optimizing hybrid electric microcar design: a simulation-based approach to fuel-cell powertrains analysis. J Phys, Conf Ser Nov. 2024;2893(1):012080. https://doi.org/10.1088/1742-6596/2893/1/012080.

[28] OPV solutions s.r.l [Online], https://opvsolutions.eu/prodotti/. [Accessed 6 December 2025].

[29] Bartolucci L, Cennamo E, Cordiner S, Donnini M, Grattarola F, Mulone V. Fuel cell hybrid electric vehicle: validated fuel cell and battery pack model to enhance reliability in performance predictions. In: Presented at the WCX SAE World Congress Experience, Detroit. United States: Michigan; Apr. 2024. https://doi.org/10.4271/2024-01-2188. 2024-01–2188.

[30] Bartolucci L, et al. Fuel cell hybrid electric vehicles: fuel cell experimental characterization and modeling towards the development of a hardware-in-the-loop platform for advanced powertrain design. J Phys, Conf Ser Dec. 2023;2648(1):012063. https://doi.org/10.1088/1742-6596/2648/1/012063.

[31] Bartolucci L, Cennamo E, Cordiner S, Krastev VK, Mulone V, Polimeni A. Metal hydrides-based hydrogen storage for light mobility applications: performance assessment through 1D numerical modeling. J Phys, Conf Ser Dec. 2025;3143(1):012076. https://doi.org/10.1088/1742-6596/3143/1/012076.

[32] Bartolucci L, Cennamo E, Cordiner S, Mulone V, Polimeni A. Hybrid renewable energy systems: integration of urban mobility through metal hydrides solution as an enabling technology for increasing self-sufficiency. Energies Oct. 2025. https://doi.org/10.3390/en18195306.

[33] Dieterich M, Pohlmann C, Bürger I, Linder M, Röntzsch L. Long-term cycle stability of metal hydride-graphite composites. Int J Hydrogen Energy Dec. 2015;40(46):16375–82. https://doi.org/10.1016/j.ijhydene.2015.09.013.

[34] Zohra FT, Webb CJ, Gray E MacA. Degradation of intermetallic hydrogen storage alloys under isochoric thermal cycling: heat-pump-like conditions. Int J Hydrogen Energy Mar. 2026;220:154174. https://doi.org/10.1016/j.ijhydene.2026.154174.

[35] AMG Titanium - GfE Metalle und Materialien GmbH. Hydralloy® C datasheet [Online], https://www.gfe.com/02_produkte_loesungen/01_legierungen/PDB/HYDRALLOY-C_2019-929_-2005-169_2004-732-_V8.pdf. [Accessed 19 February 2025].

[36] Kölbig M, Bürger I, Linder M. Thermal applications in vehicles using Hydralloy C5 in single and coupled metal hydride systems. Appl Energy Apr. 2021;287:116534. https://doi.org/10.1016/j.apenergy.2021.116534.

[37] h2planet. MyH2 3000 - cilindro per lo stoccaggio H2 in idruri metallici [Online], https://www.h2planet.eu/it/detail/MyH23000. [Accessed 19 February 2025].

[38] Brown T, Brouwer J, Samuelsen G, Holcomb F, King J. Accurate simplified dynamic model of a metal hydride tank. Int J Hydrogen Energy Oct. 2008;33(20):5596–605. https://doi.org/10.1016/j.ijhydene.2008.05.104.

[39] Bartolucci L, Krastev VK. On the thermal integration of metal hydrides with phase change materials: numerical simulation developments towards advanced designs. In: Presented at the Conference on Sustainable Mobility, Catania, Italy; Sep. 2022. https://doi.org/10.4271/2022-24-0018. 2022-24–0018.

[40] Voller VR, Prakash C. A fixed grid numerical modelling methodology for convection-diffusion mushy region phase-change problems. Int J Heat Mass Tran 1987;30.

[41] Voller VR, Swaminathan CR. ERAL source-based method for solidification phase change. Numer Heat Tran, Part B: Fundamentals Jan. 1991;19(2):175–89. https://doi.org/10.1080/10407799108944962.